Noname manuscript No.
(will be inserted by the editor)

Combination of GOCE gravity gradients in regional gravity field modelling using radial basis functions

Verena Lieb · Johannes Bouman · Denise Dettmering · Martin Fuchs · Michael Schmidt

Received: date / Accepted: date

Abstract The satellite gravity mission GOCE measured the second-order derivatives of the Earth's gravitational potential with high accuracy. The GOCE data enrich our gravity field knowledge especially at spatial resolutions from 750km down to 80km. In this paper we carry out regional gravity field analysis using radial localising basis functions that permit the combination of different data types tailored to their accuracy and spectral signal content. We formulate observation equations for each individual GOCE gravity gradient as they are distinctive reflections of the gravity field and contain directional information. To optimally use the original GOCE measurements, we derive the mathematical expressions in the gradiometer reference frame. The expressions and their implementation are validated for a test area in Scandinavia by comparison with the global gravity field model GOCO03s, which yields small differences of less than $\pm$ 1 mE. The relative weighting of the observations is determined by variance component estimation. Moreover manually fixing the weights leads to smaller residuals with respect to GOCO03s, which is probably caused by systematic errors in the gradients. We demonstrate the capabilities of our method through a combination of the gradient data with terrestrial free-air anomalies. At spatial resolutions down to 40 km the terrestrial data get much larger relative weights than the GOCE data, which indicates the proper performance of the combination method.

Keywords GOCE gravity gradients · regional gravity field modelling · radial basis functions · relative weighting · data combination

Verena Lieb
Deutsches Geodätisches Forschungsinstitut (DGFI)
Tel.: +49-89-23031-1216
E-mail: lieb@dgfi.badw.de

1 Introduction

Equipped with a 3-axis gradiometer the satellite mission GOCE (Gravity field and steady-state Ocean Circulation Explorer) (Rummel et al., 2002) observed all second-order derivatives of the Earth's gravitational potential. The gravity gradient tensor contains the complete curvature information of the local gravity field, with the advantage over the 1D gravity field information from GRACE (Gravity Recovery And Climate Experiment) (Tapley et al., 2004) that it can be applied in high-resolution gravity field determination (Pail et al., 2011), but also contains directional information allowing the gradients to be used for Earth interior research and for geophysical exploration (Ebbing et al., 2013).
An advantage of regional over global gravity field analysis is that one can adapt to local data availability and signal content. Well-established methods exist such as least-squares collocation (Tscherning and Arabelos, 2011) or spherical splines (Eicker et al., 2007). We apply radial basis functions enabling a consistent spectral combination of different observation types in order to create regional gravity fields containing maximum degree of information (Schmidt et al., 2007). The main focus in this paper lies on setting up the observation equations for the GOCE gradients in the gradiometer reference frame (GRF), which was not done so far for this method. Variance component estimation (VCE) offers the possibility of combining all 6 GOCE gradients in a flexible way: less accurate measurements can be down-weighted or excluded.
The GOCE measurement technique and the data set that is used are described in Section 2. The modelling approach itself consists of analysis and synthesis procedures which are explained in detail in Section 3. In Section 4 the results are presented and the relative

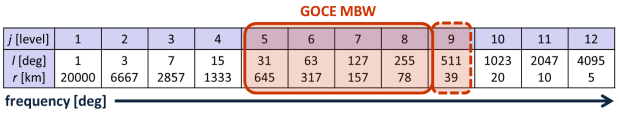

Fig. 1 Extract of the frequency spectrum which is split into resolution levels j: upper boundary corresponds to a maximum degree l spatial resolution r. Levels where GOCE has its highest sensitivity are indicated in red (MBW).

weighting of the input data is discussed. We validated the regional models with a global model. Furthermore the modelling approach can be extended by combining GOCE observations with other observation types. We present an example for the combination with high resolution free-air anomalies.

2 Gravity gradient measurements from GOCE

We use the reprocessed release 2 of GOCE observations (level-2 products), available through the GOCE Virtual On-line Archive[1]. Three pairs of accelerometers measured the gradients in the Cartesian GRF with its xyz axes pointing approximately along-track, cross-track and in radial direction. The 3×3 gravity gradient tensor is

$$\mathbf{V}_{ab} = \begin{bmatrix} V_{xx} & V_{xy} & V_{xz} \\ V_{yx} & V_{yy} & V_{yz} \\ V_{zx} & V_{zy} & V_{zz} \end{bmatrix} \tag{1}$$

with $V_{xy} = V_{yx}$, $V_{xz} = V_{zx}$, $V_{yz} = V_{zy}$, $a, b \in \{x, y, z\}$ and trace $(\mathbf{V}_{ab}) = 0$. V_{xy} and V_{yz} are less accurate than the other components and a rotation of the GOCE observations would reduce the accuracy in the rotated frame (Bouman, 2007; Fuchs and Bouman, 2011). We use observations from 02/2010 until 05/2012. The gradient errors are lowest in the measurement bandwidth (MBW) between 5 mHz and 100 mHz, above and below the MBW the errors increase rapidly. As the low part of the frequency spectrum is less accurately observed, it is removed by high-pass filtering with a cut-on frequency at the lower boundary of the MBW and filled up with model information from GOCO03s (Mayer-Gürr et al., 2012) to obtain a complete data set. Furthermore outliers and less accurate measurements have been removed.

3 Regional gravity field modelling approach

Our regional gravity field modelling approach uses radial basis functions that act as low-pass filters. They are related to specific frequency bands denoted as resolution levels j (Fig. 1). The basis functions can be expressed in terms of Legendre polynomials P_l (cf. Eq. (2)) developed up to a certain degree $l = l'_j$. This degree is related to the upper boundary of the corresponding level j with $l'_j = 2^j - 1$, representing the cut-off frequency of the low-pass filter. The degree is related to the spatial resolution at the Earth's surface as $r \approx 20000\,\mathrm{km}/l'_j$. Higher levels allow to model higher spatial resolutions contained in the gravity data.
In our approach we start with the choice of an appropriate level $j = J + 1$ related to the resolution r of the input data. Next we set up the the basis functions ϕ_{J+1} of level $J + 1$ which remove the high frequencies of the input data above degree l'_{J+1} (Schmidt et al., 2007). Finally we approximate gravitational potential differences ΔV between the potential V and an appropriate global background model, in order to represent high frequency deviations for specified regions. The series expansion in terms of scaling functions ϕ_{J+1} and scaling coefficients $d_{J,q}$ reads

$$\begin{aligned} \Delta V(\mathbf{x}^p) &= \sum_{q=1}^{N_J} d_{J,q}\, \phi_{J+1}\left(\mathbf{x}^p, \mathbf{x}_q\right) \\ &= \sum_{q=1}^{N_J} \sum_{l=0}^{l'_{J+1}} \frac{2l+1}{4\pi} d_{J,q} \Phi_{J+1,l} \left(\frac{R}{r}\right)^{l+1} P_l\left(\cos\psi\right) \end{aligned} \tag{2}$$

for an observation point $P\left(\mathbf{x}^p\right)$ with position vector $\mathbf{x}^p = r\,\mathbf{r}^p$. Herein $r = |\mathbf{x}^p|$ means the radial distance and $\mathbf{r}^p = (\cos\theta\cos\lambda, \cos\theta\sin\lambda, \sin\theta)^T$ is the unit vector depending on spherical longitude λ and co-latitude θ. The number N_J of unknown scaling coefficients $d_{J,q}$ $(q = 1, \ldots, N_J)$ and thus the number of computation points $Q\left(\mathbf{x}_q\right)$ on which the functions ϕ_{J+1} are located depends on the level $J+1$. In Eq. (2) $\Phi_{J+1,l}$ are the Legendre coefficients, R is the mean Earth radius and ψ is the spherical distance between point P and Q (Schmidt et al., 2007). Eq. (2) is given in a Terrestrial Reference Frame (TRF) in spherical coordinates, whereas the GOCE gravity gradients are measured in the Cartesian GRF. Consequently, the second-order derivatives of Eq. (2) are needed and have to be transformed into the GRF.

3.1 Adopted scaling functions

The 6 different space dependent GOCE gravity gradients in Eq. (1) are treated as 6 separate measurements and thus $K = 6$ observation equations have to be for-

[1] eo-virtual-archive1.esa.int/Index.html

mulated. The elements ΔV_{ab} can be expressed by

$$\Delta V_{ab} = \frac{\partial^2 \Delta V}{\partial a\, \partial b} = \sum_{q=1}^{N_J} d_{J,q}\, \phi_{J+1,ab}\left(\mathbf{x}^p, \mathbf{x}_q\right) \tag{3}$$

for level $J+1$ according to Eq. (2). The adopted scaling functions $\phi_{j,ab}\left(\mathbf{x}^p, \mathbf{x}_q\right)$ read for level $j \leq J+1$

$$\phi_{j,xx} = \sum_{l=0}^{l'_j} \frac{2l+1}{4\pi} \left(\frac{R}{r}\right)^{l+1} \Phi_{j,l} \cdot \left(\frac{1}{r} P_l\left(\cos\psi\right) \left(-\frac{l+1}{r}\right) + \frac{1}{r^2} \frac{\partial P_l\left(\cos\psi\right)}{\partial \theta^2}\right) \tag{4}$$

$$\phi_{j,xy} = \sum_{l=0}^{l'_j} \frac{2l+1}{4\pi} \left(\frac{R}{r}\right)^{l+1} \Phi_{j,l} \cdot \left(\frac{1}{r^2 \sin\theta} \frac{\partial P_l\left(\cos\psi\right)}{\partial \lambda \partial \theta} - \frac{1}{r^2 \sin^2\theta} \frac{\partial P_l\left(\cos\psi\right)}{\partial \lambda}\right) \tag{5}$$

$$\phi_{j,xz} = \sum_{l=0}^{l'_j} \frac{2l+1}{4\pi} \left(\frac{R}{r}\right)^{l+1} \Phi_{j,l} \cdot \left(\frac{1}{r^2} \frac{\partial P_l\left(\cos\psi\right)}{\partial \theta} - \frac{1}{r} \left(-\frac{l+1}{r}\right) \frac{\partial P_l\left(\cos\psi\right)}{\partial \theta}\right) \tag{6}$$

$$\phi_{j,yy} = \sum_{l=0}^{l'_j} \frac{2l+1}{4\pi} \left(\frac{R}{r}\right)^{l+1} \Phi_{j,l} \cdot \left(\frac{1}{r} P_l\left(\cos\psi\right) \left(-\frac{l+1}{r}\right) + \frac{1}{r^2 \tan\theta} \frac{\partial P_l\left(\cos\psi\right)}{\partial \theta} + \frac{1}{r^2 \sin^2\theta} \frac{\partial P_l\left(\cos\psi\right)}{\partial \lambda^2}\right) \tag{7}$$

$$\phi_{j,yz} = \sum_{l=0}^{l'_j} \frac{2l+1}{4\pi} \left(\frac{R}{r}\right)^{l+1} \Phi_{j,l} \cdot \left(\frac{1}{r^2 \sin\theta} \frac{\partial P_l\left(\cos\psi\right)}{\partial \lambda} - \frac{1}{r \sin\theta} \left(-\frac{l+1}{r}\right) \frac{\partial P_l\left(\cos\psi\right)}{\partial \lambda}\right) \tag{8}$$

$$\phi_{j,zz} = \sum_{l=0}^{l'_j} \frac{2l+1}{4\pi} \left(\frac{R}{r}\right)^{l+1} \Phi_{j,l} \cdot P_l\left(\cos\psi\right) \frac{(l+1)(l+2)}{r^2}. \tag{9}$$

Similar expressions can be derived for other radial basis functions, as e.g. covariance functions (Tscherning, 1993) or spherical splines (Eicker et al., 2007).

3.2 Analysis

The reduced GOCE gradients are treated as separate observations assuming that we have no error correlations. The observation equation reads for one tensor element ΔV_{ab}, observed at the observation points $\mathbf{x}^p$ with $p \in \{1, \ldots, P\}$ according to Eq. (3) and considering the measurement error e_{ab}

$$\Delta V_{ab}\left(\mathbf{x}^p\right) + e_{ab}\left(\mathbf{x}^p\right) = \boldsymbol{\phi}_{ab}^T\left(\mathbf{x}^p\right) \mathbf{d}_J. \tag{10}$$

$\boldsymbol{\phi}_{ab}$ is the $N_J \times 1$ vector of modified scaling functions according to Eqs. (4) to (9). In the analysis step we use the Shannon scaling function with the Legendre coefficients $\Phi^{\mathrm{SHA}}_{J+1,l} = 1$, which is an ideal low-pass filter up to degree l'_{J+1} (Schmidt et al., 2007). Rotating the resulting expressions into GRF leads to the observation equations of the tensor in GRF. The $N_J \times 1$ vector $\mathbf{d}_J = \left[d_{J,1}, \ldots, d_{J,N_J}\right]^T$ of scaling coefficients is then estimated by VCE as will be briefly explained in the following. We collect all measurements of a particular gravity gradient, so that each observation group $\boldsymbol{\Delta}\mathbf{v}_k$ with $k \in \{1, \ldots, K\}$ represents a $P \times 1$ vector of the measurements ΔV_{ab} and $\boldsymbol{\phi}_k$ represent the corresponding $P \times N_J$ matrices of scaling functions:

$$\begin{bmatrix} \boldsymbol{\Delta}\mathbf{V}_{xx} \\ \boldsymbol{\Delta}\mathbf{V}_{xy} \\ \boldsymbol{\Delta}\mathbf{V}_{xz} \\ \boldsymbol{\Delta}\mathbf{V}_{yy} \\ \boldsymbol{\Delta}\mathbf{V}_{yz} \\ \boldsymbol{\Delta}\mathbf{V}_{zz} \end{bmatrix} = \begin{bmatrix} \boldsymbol{\Delta}\mathbf{v}_1 \\ \boldsymbol{\Delta}\mathbf{v}_2 \\ \boldsymbol{\Delta}\mathbf{v}_3 \\ \boldsymbol{\Delta}\mathbf{v}_4 \\ \boldsymbol{\Delta}\mathbf{v}_5 \\ \boldsymbol{\Delta}\mathbf{v}_6 \end{bmatrix} = \boldsymbol{\Delta}\mathbf{v} \quad \text{and} \quad \begin{bmatrix} \boldsymbol{\phi}_1 \\ \boldsymbol{\phi}_2 \\ \boldsymbol{\phi}_3 \\ \boldsymbol{\phi}_4 \\ \boldsymbol{\phi}_5 \\ \boldsymbol{\phi}_6 \end{bmatrix} = \boldsymbol{\phi}. \tag{11}$$

For the combination of GOCE gradient observations with further measurement techniques the vector $\boldsymbol{\Delta}\mathbf{v}$ can be extended by other observation groups $\boldsymbol{\Delta}\mathbf{v}_k$ with $k > K$. The stochastic part is formulated as

$$\mathbf{D}\left(\begin{bmatrix} \boldsymbol{\Delta}\mathbf{v}_1 \\ \boldsymbol{\Delta}\mathbf{v}_2 \\ \boldsymbol{\Delta}\mathbf{v}_3 \\ \boldsymbol{\Delta}\mathbf{v}_4 \\ \boldsymbol{\Delta}\mathbf{v}_5 \\ \boldsymbol{\Delta}\mathbf{v}_6 \\ \boldsymbol{\mu}_d \end{bmatrix}\right) = \begin{bmatrix} \sigma_1^2 \mathbf{P}_1^{-1} & \mathbf{0} & \ldots & \mathbf{0} \\ \mathbf{0} & \sigma_2^2 \mathbf{P}_2^{-1} & \ldots & \mathbf{0} \\ \vdots & \vdots & \ddots & \vdots \\ \mathbf{0} & \mathbf{0} & \ldots & \sigma_d^2 \boldsymbol{\Sigma}_d \end{bmatrix}. \tag{12}$$

$\mathbf{D}$ is the covariance matrix, $\mathbf{P}_k$ is the $P \times P$ weighting matrix of the observation vector $\boldsymbol{\Delta}\mathbf{v}_k$. Note, the background model is introduced as additional observation to avoid singularity problems. Referred to Schmidt et al. (2007) the vector $\boldsymbol{\mu}_d$ contains the expectation values of the coefficients from the background model and $\boldsymbol{\Sigma}_d$ is the corresponding $N_J \times N_J$ covariance matrix. The variance components (VC) σ_k^2 and σ_d^2 are determined iteratively according to Koch and Kusche (2002). With the estimated VCs the estimated coefficients $\widehat{\mathbf{d}}_J$ result in

$$\widehat{\mathbf{d}}_J = \left(\sum_{k=1}^{6} \frac{1}{\widehat{\sigma}_k^2} \boldsymbol{\phi}_k^T \mathbf{P}_k \boldsymbol{\phi}_k + \frac{1}{\widehat{\sigma}_d^2} \boldsymbol{\Sigma}_d^{-1}\right)^{-1} \cdot \left(\sum_{k=1}^{6} \frac{1}{\widehat{\sigma}_k^2} \boldsymbol{\phi}_k^T \mathbf{P}_k \boldsymbol{\Delta}\mathbf{v}_k + \frac{1}{\widehat{\sigma}_d^2} \boldsymbol{\mu}_d\right). \tag{13}$$

The estimated covariance matrix of the coefficients reads $\mathbf{Q}_{dd} = \left(\sum_{k=1}^{6} \frac{1}{\widehat{\sigma}_k^2} \boldsymbol{\phi}_k^T \mathbf{P}_k \boldsymbol{\phi}_k + \frac{1}{\widehat{\sigma}_d^2} \boldsymbol{\Sigma}_d^{-1}\right)^{-1}$.

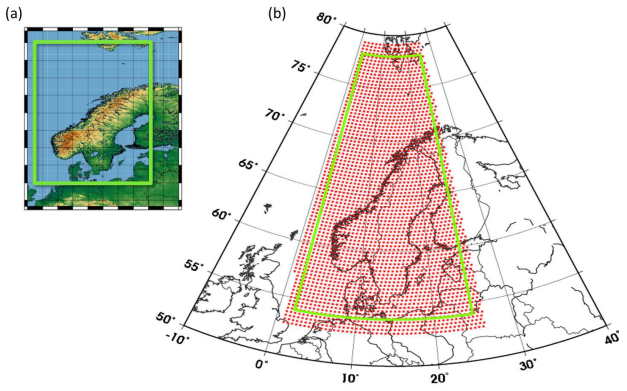

Fig. 2 (a) Geographical location of the test area Scandinavia (green bordered) with altitude encoding topography. (b) Distribution of the grid points (red dots).

3.3 Synthesis

For the synthesis step we set up the series expansions (3) in terms of Blackman scaling functions $\phi_{J+1,ab}$, characterized by the Legendre coefficients $\Phi^{\mathrm{BLA}}_{J+1,l}$ (Schmidt et al., 2007). Compared with the Shannon kernel the functions act also band-limiting as low-pass filters up to degree l'_{J+1} according to Fig. 1, but with a smoother declining behavior. Consequently, in the spatial domain the oscillations and sidelobes of the Blackman functions are much smaller. Thus erroneous edge effects are significantly reduced. Inserting the estimated coefficients $\widehat{\mathbf{d}}_J$ (cf. Eq. (13)) into Eq. (3) and using Eqs. (4) to (9) with $\Phi^{\mathrm{BLA}}_{J+1,l}$ yields the estimated gradients of the reduced gravitational potential.

4 Numerical investigations

4.1 Study area and modelling parameters

We study the Scandinavian region with an extent of 2° to 25° in longitude and 54° to 78° in latitude, see Fig. 2(a). The frequency part where GOCE measures with its highest sensitivity can be seen from Fig. 1. It is highlighted in red and indicates a spatial resolution down to ~ 80 km. Level $j = 8$ is the maximum level which is completely located within the sensitivity domain of GOCE, whereas the upper part of level 9 contains a lot of noise so that only the low frequencies of $j = 9$ deliver significant information. For our numerical investigations we consequently use the modelling approach up to level $J + 1 = 8$. The level depending computation points of the scaling functions can be seen in Fig. 2(b) (red dots). The computation area has a larger extent than the modelling area (green bordered) to diminish edge effects. The observation area containing the GOCE satellite tracks has an extension in-between both margins. Furthermore the data set is reduced by the global background model GOCO03s up to maximum degree and order 250 following Eq. (3). We used exactly the same model as for filling up the low frequencies to be consistent. The resolution of GOCO03s reaches nearly to the modelling resolution at level 8, so that most of the signal is reduced and only small deviations remain which are approximated in the estimation process.
Inserting the reduced GOCE gradients in the observation equation (10), assuming that the measurement errors are uncorrelated and have the same accuracies within an observation group k, allows us to introduce identity matrices for the weighting matrices $\mathbf{P}_k$ in Eq. (12). As prior information we use the same model as the background model (GOCO03s). Consequently we assume that the $N_J \times 1$ vector $\boldsymbol{\mu}_d$ is equal to $\mathbf{0}$ and the covariance matrix $\boldsymbol{\Sigma}_d$ corresponds to the identity matrix.

4.2 Gradient grids

As output from the synthesis procedure we obtain approximation signals which can be expressed as any functional of the gravitational potential (e.g. geoid undulations N, gravity anomalies Δg). Restoring the background model, subtracting the normal potential from the reference ellipsoid WGS84 and computing the second-order derivatives V_{ab} lead to the gradients of the disturbing potential T_{ab} for all combinations of the xyz Cartesian coordinates. Figure 3 shows the results according to the xyz tensor arrangement in a local-north-oriented frame with its axes pointing north-, west- and upwards. The modelling height corresponds to the mean GOCE orbit height of 270 km within this region. The gradients of the disturbing potential show clearly different structures depending on the different spatial directions. As expected, the radial zz component pointing directly along the field line of the Earth's gravitational potential has the largest magnitudes between $\pm\,0.5$ E. The sum of the diagonal elements should be zero according to the Laplace condition $\mathrm{trace}\,(\mathbf{T}_{ab}) = 0$. The trace criteria gives values which are 3 orders of magnitude smaller than the signals of the single components. Considering the modelling accuracy, which depends on edge effects, oscillations of the scaling functions, smoothing and interpolation effects, the Laplace condition is therefore fulfilled. The approximation signals without restoring the background model GOCO03s vary between ± 1 mE containing additional signal to the global model but also errors from the regional approach.

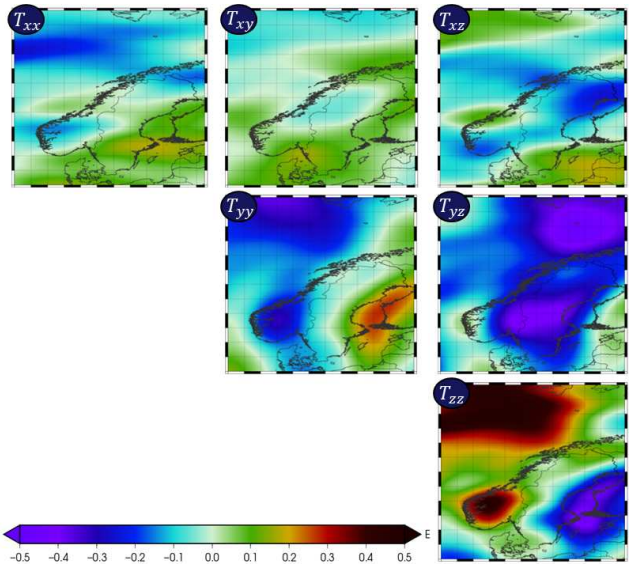

Fig. 3 Gravity gradient grids of the second-order derivatives of the disturbing potential modelled from GOCE gradient measurements at 270 km height.

4.3 Analysis of VCE

Variance component estimation provides a flexible tool for relative weighting of different observation groups by combining them at the level of observation equations. A large VC σ_k^2 means hereby a low relative weight of the observation group $\mathbf{\Delta v}_k$ in Eq. (13). Table 1, col. (a) lists the orders of magnitude of the iteratively estimated VCs with reference to V_{zz}. The diagonal component V_{xx} obtains the same weight as the radial pointing V_{zz}. It has a smaller signal content, but also a twice smaller noise level, so that similar weighting seems to be appropriate. The less accurate components V_{xy} and V_{yz} are down-weighted by 2 and 5 orders of magnitude, respectively. Thus some information from V_{xy} is still present in the solutions while the influence of V_{yz} is negligible. The prior information is down-weighted by 2 orders of magnitude indicating that it contributes also to the output grids. The down-weighting is justified in the errors of the long wavelengths part of GOCO03s which cannot be accounted for. Against the expectation that the 4 accurate GOCE gradients should have comparable weights, V_{xz} gets a lower weight signifying that this gradient component is less accurate than the diagonal elements. We assume that this effect is specific for the Scandinavian region, as studies in other regions deliver similar VCs for the 4 components.
V_{yy} gets the same weight as the diagonal components V_{xx} and V_{zz}, but as our test area is located near the North pole we further have to deal with systematic errors in this component (Bouman et al., 2011; Bouman and Fuchs, 2012). In a second computation we thus manually fixed the relative weights (Table 1, col. (b)): the VCs of V_{xx} and V_{zz} are adapted to the estimated values, but V_{yy} is down-weighted by 5 orders of magnitude. We assume a noise behaviour comparable with that of V_{yz} obtained in the estimated case. V_{xy} and V_{yz} are additionally down-weighted. Using those fixed weights we apply least squares estimation within a Gauss-Markov model. We compare the results from both weighting strategies with the global GOCO03s model. The mean standard deviation of the difference grids decreases from 0.1 mE (for estimated VCs) down to 0.03 mE when setting a lower relative weight for V_{yy} component. In our study area the differences decline especially in the northern part at latitudes $> 70°$. We conclude that this might be due to the down-weighted impact of V_{yy} and plan to investigate further studies.

Table 1 Relative weighting of observations. Given are the orders of magnitude of the related VCs σ_k^2 [–].

observation	(a) est	(b) fix	(c) fix
GOCO03s	10^2	10^2	10^2
V_{xx}	1	1	1
V_{xy}	10^2	10^{13}	10^8
V_{xz}	10^3	10^2	10^2
V_{yy}	1	10^5	10^5
V_{yz}	10^5	10^{13}	10^8
V_{zz}	1	1	1
FA			10^{-2}

4.4 Combination with free-air anomalies

Finer structures can be modelled by combining GOCE gravity gradients with high-resolution data sets such as free-air anomalies (FA). Figure 4 shows gravity anomalies with variations between ± 100 mGal at the Earth's surface obtained from a combination at level 9 ($l' = 511$). Compared with GOCE, the FA data set (Olesen et al., 2010a,b) contains detailed information from altimetry, terrestrial and shipborne gravimetry. The FA data therefore get a higher weight than the GOCE V_{zz} gradients (2 orders of magnitude, determined with VCE). Table 1, col. (c) shows the corresponding manually fixed weights of all input data sets. The lower frequency domain of the solution is stabilised by the GOCE observations. For areas where high-frequency data are available, our regional gravity field modelling approach offers the opportunity to combine data sets which are sensitive to different frequency domains by VCs such, that the data with the highest signal content up to a specific level j contribute the most. In contrast to other gravity analysis techniques weights can be introduced individually for each resolution level.

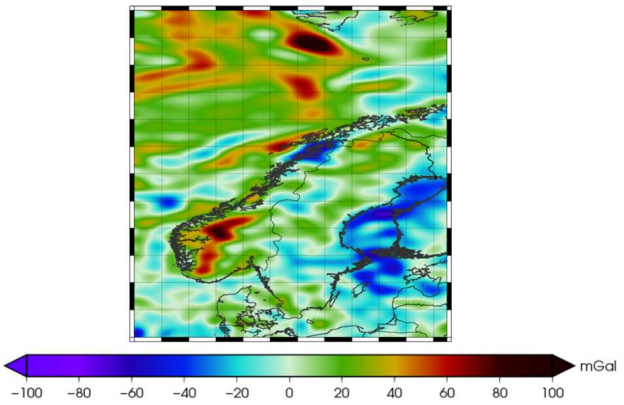

Fig. 4 Combination of GOCE gravity gradients and free-air anomalies (FA) at level 9 ($j' = 511$) using manually fixed relative weights, Table 1 (c).

5 Summary

We derived the observation equations for GOCE gravity gradient measurements in a regional gravity field modelling approach using radial basis functions. Our aim was to use the original GOCE gravity gradients in the GRF to maintain the precision of the 4 accurate components. The resulting gradient grids show different structures that give information of the Earth's gravitational potential depending on different spatial directions. This advantage might further be used for research on the Earth's interior and for geophysical exploration (Ebbing et al., 2013). A validation of our regional gradients grids with GOCO03s gives differences that are smaller than $\pm\,1$ mE, which confirms that our method works properly. We also found that the use of VCs for the automatic estimation of the relative weights of the different gradient components may not be optimal. Manually down-weighting the less accurate V_{xy} and V_{yz} components as well as down-weighting the regionally less accurate V_{yy} component, significantly reduces the differences to the global GOCO03s model. Thus the optimal combination of the gradient data sets requires further study, especially in the presence of systematic errors as may be the case for V_{yy}. Moreover we demonstrated a combination of the GOCE gravity gradients with high-resolution FA anomalies. The latter enable to model more detailed structures at higher resolution levels. With this additional information radial basis functions might offer the possibility to enrich and supplement global gravity fields in specified regions.

Acknowledgements The authors want to thank the European Space Agency (ESA) for funding the project GOCE+ GeoExplore. Further we are grateful to P. Willis, C.C. Tscherning and two anonymous reviewers for their valuable input.

References

Bouman J., Alternative method for rotation to TRF. GO-TN-HPF-GS-0193, ESA-ESTEC, Noordwijk (2007)

Bouman J., Fiorot S., Fuchs M., Gruber T., Schrama E., Tscherning C.C., Veicherts M., Visser P., GOCE gravitational gradients along the orbit. J Geod 85(11), 791-805, doi 10.1007/s00190-011-0464-0 (2011)

Bouman J., Fuchs M., GOCE gravity gradients versus GOCE gravity field models, Geophys. J. Int. 189(2), 846-850, doi 10.1111/j.1365-246X.2012.05428.x (2012)

Ebbing J., Bouman J., Fuchs M., Lieb V., Haagmans R., Meekes S., Abdul Fattah R., Advancements in satellite gravity gradient data for crustal studies, The Leading Edge 32, 900-906, doi 10.1190/tle32080908.1 (2013)

Eicker A., Mayer-Gürr T., Ilk K.H., A global CHAMP gravity field by merging of regional refinement patches. Proceedings Joint CHAMP/GRACE Science Team Meeting 2004, 0000:00015 (2007)

Fuchs M., Bouman J., Rotation of GOCE gravity gradients to local frames. Geophys. J. Int. 187(2), 743-753, doi 10.1111/j.1365-246X.2011.05162.x (2011)

Koch K.R., Kusche J., Regularization of geopotential determination from satellite data by variance components. J Geod 76, 259-286, doi 10.1007/s00190-002-0245-x (2002)

Mayer-Gürr T., Rieser D., Höck E., Brockmann J..M., Schuh W.-D., Krasbutter I., Kusche J., Maier A., Krauss S., Hausleitner W., Baur O., Jäggi A., Meyer U., Prange L., Pail R., Fecher T., Gruber T., The new combined satellite only model GOCO03s. Symposium on Gravity, Geoid and Height Systems (talk), Venice, October 9-12 (2012)

Olesen O., Brünner M., Ebbing J., Gellei, J., Gernigon L., Koziel J., Lauritsen T., Myklebust R., Sand M., Solheim D., Usov S., New aeromagnetic and gravity compilations from Norway and adjacent areas methods and applications. Petroleum Geology Conf series 7, 559-586 (2010a)

Olesen O., Ebbing J., Gellein J., Kihle O., Myklebust R., Sand M., Skilbrei J.R., Solheim D., Usov S., Gravity anomaly map, Norway and adjacent areas. Geological Survey of Norway (2010b)

Pail R., Bruinsma S., Migliaccio F., Förste C., Goiginger H., Schuh W.D., Hoeck E., Reguzzoni M., Brockmann J.M., Abrikosov O., Veicherts M., Fecher T., Mayrhofer R., Krasbutter I., Sansò F., Tscherning C.C., First GOCE gravity field models derived by three different approaches. J Geod 85, 819-843, DOI: 10.1007/s00190-011-0467-x (2011)

Rummel R., Balmino G., Johannessen J., Visser P., Woodworth P., Dedicated gravity field missions - principle and aims. J Geodyn 33(1-2), 3-20, doi 10.1016/S0264-3707(01)00050-3 (2002)

Schmidt M., Fengler M., Mayer-Gürr T., Eicker A., Kusche J., Sánchez L., Han S.-C., Regional gravity modelling in terms of spherical base functions. J Geod 81(1), 17-38, doi 10.1007/s00190-006-0101-5 (2007)

Tapley B.D., Bettadpur S., Watkins M., Reigber C., The gravity recovery and climate experiment: Mission overview and early results, Geophys. Res. Lett., 31, L09607, doi:10.1029/2004GL019920 (2004)

Tscherning C.C., Computation of covariances of derivatives of the anomalous gravity potential in a rotated reference frame. Manuscripta Geodaetica 18(3), 115-123 (1993)

Tscherning C.C., Arabelos D.N., Gravity anomaly and gradient recovery from GOCE gradient data using LSC and comparisons with known ground data. Proc. 4th Int. GOCE user workshop, ESA SP-696, March 31 - April 1 (2011)